Front. Earth Sci. 2023, 17(4): 981–996
https://doi.org/10.1007/s11707-022-1049-3

RESEARCH ARTICLE

Detecting the spatial-temporal pattern of moisture evolution on the Tibetan Plateau during the Holocene by model-proxy comparison

Zeyu ZHENG[1], Liya JIN (✉)[2,1], Jinjian LI[2,1], Xiaojian ZHANG[3], Jie CHEN[1]

1 MOE Key Laboratory of Western China's Environmental System, College of Earth and Environmental Sciences, Lanzhou University, Lanzhou 730000, China
2 School of Atmospheric Sciences, Chengdu University of Information Technology, Chengdu 610225, China
3 School of Geographic and Oceanographic Sciences, Nanjing University, Nanjing 210023, China

Abstract The Tibetan Plateau (TP) is a key region for environmental and climatic research due to its significant linkages with large-scale atmospheric circulation. Understanding the long-term moisture evolution pattern and its forcing mechanisms on the TP during the Holocene may provide insights into the interaction between low-latitude climate systems and midlatitude westerlies. Here, we synthesized 27 paleoclimate proxy records covering the past 9500 years. The results of the rotated empirical orthogonal function analysis of the moisture variation revealed spatial-temporal heterogeneity, which was classified into 5 subregions. Proxy records were then compared with the results from the Kiel Climate Model and other paleorecords. The results showed that moisture evolution on the western-southern-central TP was controlled by the Indian summer monsoon (ISM). On the south-eastern TP, moisture change was affected by the interplay between the East Asian summer monsoon (EASM) and the westerlies, as well as the ISM. With diverse patterns of circulation system precipitation, moisture changes recorded in the paleorecords showed spatial-temporal discrepancies, especially during the early to middle Holocene. Moreover, given the anti-phase pattern of summer precipitation in the EASM area under El Niño/Southern Oscillation (ENSO) conditions and the unstable relationship between the ISM and ENSO, it is reasonable to conclude that relatively strong ENSO variability during the late Holocene has contributed to these discrepancies as Asian summer monsoon precipitation has declined.

Keywords Tibetan Plateau, Holocene, moisture evolution, model-proxy comparison

Received October 10, 2022; accepted January 29, 2023

E-mail: jinly@lzu.edu.cn

1 Introduction

Understanding climate changes since the last glacial period is a key point in paleoclimate research, especially those impacting the Asian summer monsoon (ASM; including the East Asian summer monsoon (EASM) and Indian summer monsoon (ISM)) climate and westerlies climate, which are two pivotal circulation components of global circulation systems (Kutzbach, 1981; Oldfield, 1999; Chen et al., 2016). The TP stretches over 3.08×10^6 km^2 and has an average elevation of approximately 4320 m above sea level (m a.s.l.) in mid-latitude regions (Zhang et al., 2002, 2021); Previous researches have revealed that the TP is of great significance for the climate of Asia, as it not only influences the intensity of the EASM and the ISM by altering the land–sea thermal contrast and the circulation coupling between both the subtropics and tropics and the lower and upper troposphere (Liang et al., 2006; Wu et al., 2012; Tada et al., 2016) but also affects the intensity and location of the westerly jet in the spring (Li and Liu, 2015). Thus, unique location and configuration enable the TP climatically sensitive and ideal for paleoclimate research (Zhu et al., 2009; Cheng et al., 2013).

In recent decades, a number of paleorecords from the TP have been used to reconstruct past climates, thereby improving our understanding of climate change during the Holocene and extends the spatial coverage of environmental records for the TP (He et al., 2004; Herzschuh et al., 2006; Zhu et al., 2015). Additionally, some studies have tried to detect the climate evolution pattern over the TP. However, the complexity in topography and inner terrain elevation differences, as well as the interplay among the dominant circulation systems, i.e., EASM, ISM, and midlatitude westerlies,

make it difficult to draw conclusions about the spatial and temporal patterns of paleoclimate evolution (An et al., 2000, 2006; Yang et al., 2008). According to modern observation data, moisture flowing to the western TP is relative to the Arabian Sea, as well as the ISM (Jin, 2006). Dong et al. (2017) confirmed that ISM low-pressure systems brought large amounts of precipitation from north and central India to the south-western TP. On the northern TP, climate change is controlled by westerlies (Gao et al., 2014). Recently, based on three gridded precipitation databases over the ASM region from 1979 to 2009 and empirical orthogonal function analysis (EOF), Conroy and Overpeck (2011) suggested that rainfall seasonality followed a typical monsoon pattern, which received approximately 60% of the annual total between May and October; they then divided the modern climate on the TP region into three areas with distinct precipitation variabilities, i.e., south-east, north-west, and south-west, with the driest conditions in the north-western TP and wetter conditions in the eastern TP. These different areas were likely to have different moisture sources. The precipitation in the eastern subregion was brought by the EASM from the western North Pacific, and that in the western subregion was related to the ISM. However, the precipitation on the north-western TP might be related to continental water recycling.

When considering higher Northern Hemisphere summer insolation during the Holocene (Berger and Loutre, 1991), the existence of a spatial-temporal pattern of moisture evolution similar to the current situation has yet to gain consensus. For example, Herzschuh et al. (2006) argued that there were east–west regional differences in climate evolution and in the timing of optimal conditions, which may have resulted from the availability of the spatially fluctuating effective moisture. Chen et al. (2008) compared paleolimnological data from across the TP and confirmed that effective moisture and lake levels in monsoon-influenced TP were lower during the late Holocene, while effective moisture and lake levels in mainly westerlies-influenced areas experienced low levels in the early Holocene and high levels during the middle to late Holocene. Zhang and Mischke (2009) also supported the different spatial patterns and suggested that a possible mechanism may be the insolation-driven southward drawing of westerly winds in the early Holocene. After comparing the climate in the Nam Co area inferred from pollen data with other climates on the TP, Li et al. (2011) summarized that the temporal succession, i.e., the termination of maximum monsoon precipitation or moisture conditions occurring earlier on the western TP than on the eastern TP, followed a hypothesized south-eastward retreat of monsoon moisture during the middle to late Holocene along a modern precipitation gradient, as concluded from a monthly 1900–2014 global gridded precipitation data set. An et al. (2012) suggested that climate evolution on the north-eastern TP was controlled by the interplay between the westerlies and ASM during the Holocene. Zhu et al. (2015) and Hou et al. (2017) obtained lake sediments on the central TP and affirmed that the climate change during the Holocene was influenced mainly by the ISM. In contrast, general agreement in paleohydrological evolution on the TP during the Holocene was presented by Mügler et al. (2010) after comparing wet and dry periods inferred from 6 lake records across the TP. In addition, Wischnewski et al. (2011) applied a five-scale moisture index and average link clustering to semiquantitative moisture information to detect general patterns of moisture evolution and confirmed that there were obvious differences in moisture evolution inferred from paleoclimatic data, but it is difficult to identify coherent temporal and spatial patterns. Apart from the viewpoints outlined above, Doberschütz et al. (2014) considered that there was temporal variability in the behavior of the moisture evolution from lake sediments, which was nearly synchronous in the middle Holocene and showed a nonuniform response to climate change in the late Holocene.

Considering the considerable discrepancy regarding the climatic significance of the proxies used in lake sediments (Chen et al., 2016), the nature of Holocene climatic changes in the region could be concealed. Furthermore, few attempts have been made to clarify the circulation configurations on the TP. Consequently, in the present paper, we investigate the spatial and temporal characteristics of Holocene moisture evolution recorded in paleoclimatic records and detect whether the moisture pattern of regional heterogeneity on the TP truly remained over time during the Holocene as in the modern climate, as well as the possible forcing mechanisms. In this respect, paleoclimate modeling and its comparison with proxy records is a very useful strategy. Paleoclimate records provide an observational basis for verifying the precision of the model, which can further be used in developing and tuning numerical models. The models, once the accuracy in corresponding climate factors is confirmed, can be used to explore the dynamics that have driven climate variability in the past. Therefore, we used model data over the past 9.5 ka and compared the simulation results with moisture inferred from sediments to explore the driving factors for moisture changes over the TP during the Holocene.

2 Data and methods

2.1 Kiel Climate Model (KCM) description

The Kiel Climate Model (KCM), a state-of-the-art coupled ocean-sea-ice-atmosphere general circulation model, comprises the atmospheric general circulation model ECHAM5 and the Nucleus for European Modeling of the Ocean (NEMO) ocean-sea ice general circulation

model, using OASIS3 as a coupler. The horizontal resolution of ECHAM5 is T31 (3.75° × 3.75°), with 19 vertical levels from 1000 hPa to 10 hPa. The horizontal resolution of NEMO, using the Mercator meshes with grid refinement in the tropical regions, attains an average resolution of 1.3°. More details on the model can be found in Park et al. (2009).

The transient simulation started at 9.5 ka BP, which was output from an equilibrium simulation forced by Earth's orbital parameters, including eccentricity, obliquity and precession (Berger and Loutre, 1991). Thereafter, with a 10-fold acceleration scheme, the simulation was forced by varying the orbital parameters according to the respective period from 9.5 to 0 ka BP (Lorenz and Lohmann, 2004). Other forcing factors except insolation forcing, such as greenhouse gas concentrations, continental ice sheets and meltwater fluxes, were set at preindustrial (AD 1850) levels. A more detailed description of the model setting can be found in Jin et al. (2014).

KCM model data have been verified as an effective tool for paleoclimatic research. Jin et al. (2014) employed equilibrium and transient simulation data to probe spatial-temporal patterns over ASM and monsoon marginal regions and suggested that the synthesis of multiproxy records and model experiments were in accordance. In addition, Zhang et al. (2016) used KCM model data to investigate how summer North Atlantic sea surface temperatures (SSTs) may have influenced the ISM at centennial timescales during the Holocene (9.5−0 ka BP). Recently, Zhang et al. (2018) compared KCM transient simulation data with proxy-based precipitation changes on the north-eastern TP and confirmed the uniformity between pollen data and KCM data.

2.2 Paleoclimatic record selection

The objective of this study is to review Holocene moisture evolution and to investigate whether there is an obvious spatial-temporal moisture evolution pattern on the TP. To avoid the disparity of different paleoclimatic records in climate change, we only selected lake sediment and peat bog data to reconstruct the paleoclimate. However, with large discrepancies in sample resolution and age control among paleorecords, the patterns based on record-time-slide comparisons may be distorted. To ensure reliable data quality, we collected published data and selected the data according to criteria similar to previous studies (Herzschuh, 2006; Chen et al., 2008; Wang et al., 2010; Wang et al., 2017). 1) The record must cover at least 4000 years during the Holocene. In this paper, because we regarded 8 ka and 4 ka as the early/middle Holocene and middle/late Holocene time boundaries, respectively, a record covering at least 4000 is more precise to represent the general situation during the subperiods of the Holocene. 2) The proxies in the record must be indicative of past precipitation/moisture changes. In this study, lake sediment and peat bog data, including geophysical (lithological description, color index, grain size, etc.), geochemical (organic and inorganic carbon content, stable carbon and oxygen isotope ratios, and elemental composition), and pollen data were selected. Pollen data, which have been frequently used in climate reconstructions, are considered a reliable signal for climate changes at a regional scale (Zhao et al., 2009a, 2009b). Wang et al. (2010) used Procrustes analysis to evaluate the concordance between pollen and nonpollen and demonstrated the significant concordance between pollen and nonpollen data sets (Peres-Neto and Jackson, 2001) and synchronous signals between pollen and nonpollen records on centennial timescales, which permits us to use them together for ordination purposes. However, in this study, carbonate oxygen isotope records ($\delta^{18}O_{carb}$), which is prevalent in lacustrine research, were not collected. In some cases, lacustrine $\delta^{18}O_{carb}$ documents different climate evolution with other proxies, such as the $\delta^{18}O_{carb}$ data and pollen data in Qinghai Lake. According to Zhang et al. (2018) and Wu et al. (2022), the isotopic composition of lake water can be influenced by many factors, including temperature, evaporation, site elevation, meltwater supply, and moisture sources. Complicated influencing factors and different climate implications of $\delta^{18}O_{carb}$ make it difficult to combine with other proxies. 3) The time sequences should be based on reliable chronology, with more than four dating control points during the Holocene. 4) The sampling resolution was sufficient for this research (< 200 years for the Holocene period). All selected sites were first checked to remove any possible old carbon effect. Then, if necessary, all ^{14}C ages were calibrated to determine ages in this paper using the calibration program Calib 8.1.0, with the newest calibration curve (IntCal 20). Calibrated ages were used when compiling moisture curves throughout the paper (expressed as cal. a BP or cal. ka BP, 1 ka = 1000 cal. a BP) (Chen et al., 2008; Zhang et al., 2011). 5) The old carbon/reservoir effect was mentioned and removed in the original paper. As research shows, the old carbon/reservoir effect is universal in lakes on the TP. Hou et al. (2012) demonstrated that the old carbon/reservoir effect exhibited significant spatial and temporal variability on the TP, ranging from almost 7000 years to several years. Therein, the largest reservoir effect was in Bangong Lake (6670 years). In addition, Mischke et al. (2013) argued that the largest reservoir effect can reach 20000 ^{14}C years. To make a valid comparison, the old carbon/reservoir effect must be removed.

To obtain moisture index inference for paleoclimatic records, multiproxy anomalies at an individual lake were first calculated and normalized. According to the normalized results, the signals of moisture evolution were coded on a four-part scale developed by Herzschuh

(2006): dry (0), moderately dry (1), moderately wet (2), and wet (3). A high wetness value was assigned to intervals with fine-grained sediments, high Artemisia/Chenopodiaceae pollen ratios, high organic content and humification, low long-chain leaf wax and so on. Each moisture degree was individualized, and there was no comparability because of their geographic locations, archives, proxies used and sensitivities. Relative moisture evolution sequences indicate how the climate around the lakes/peat evolved so that we could distinguish whether all the records were influenced under the same climate system. Every sequence was conducted for each 100-year interval. However, because there might be several proxies from one site, it was impossible to consistently translate each individual proxy into semiquantitative climate signals at all sites. Therefore, after carefully crosschecking the interpretations from original papers, we largely agreed with the conclusions drawn from the authors when classifying proxy-based climatic inferences into the moisture index. The definition of the paleorecord boundaries was based on the results of REOF using FORTRAN, which overcomes the shortcomings of EOFs in presenting the characteristics of different geographical regions and is widely used in modern climate research to investigate the spatial pattern of climate evolution (Richman, 1986).

Based on the criteria mentioned above, we analyzed 27 lake sediments and 1 peat bog sediment on the TP. As inferred from the deposits and landforms of glaciers on the TP, climate change during the early Holocene was significantly unstable (Owen et al., 2005; Zhang and Mischke, 2009, 2022). For example, a climate reversal during the early Holocene probably represents the widely recognized Younger Dryas, although there are significant differences among records (Tschudi et al., 2003). Some records cannot capture these climate events, such as those events involving Koucha and Kuhai Lakes (Mischke et al., 2008, 2010). Evidence from other studies records the Younger Dryas with a time difference (12.5−11.7 ka BP from Lake Naleng and from 11.3 to 10.8 ka BP from Lake Qinghai) (Shen et al., 2005; Kramer et al., 2010a). The significant discrepancies in moisture change during the early Holocene make it difficult to perform further analysis. Therefore, to ensure the time uniformity between proxy data and model data, we studied a period spanning 9.5−0 ka BP. Herein, 21 records span the complete period between 9.5 and 0 cal. ka BP, the other 6 sediment records remained incomplete (Fig. 1 and Table 1).

3 Results

3.1 Spatial and temporal characteristics of Holocene moisture evolution on the TP

We divided the Holocene into five periods to investigate the spatial and temporal characteristics of Holocene moisture evolution on the TP. The Holocene moisture histories showed distinct spatial discrepancies (Fig. 2). During the early Holocene (9.5−8 ka), the climate was clearly wet on the western, southern, central and southeastern TP. Meanwhile, most of the sediments on the north-eastern TP experienced moderate or wet conditions. In contrast, No. 19 (Hurleg Lake) and No. 20 (Koucha Lake) recorded dry conditions. In the first half of the mid-Holocene (8−6 ka), the climate recorded in the deposits was significantly asynchronous. Most of the paleoclimatic data on the north-eastern TP recorded humid

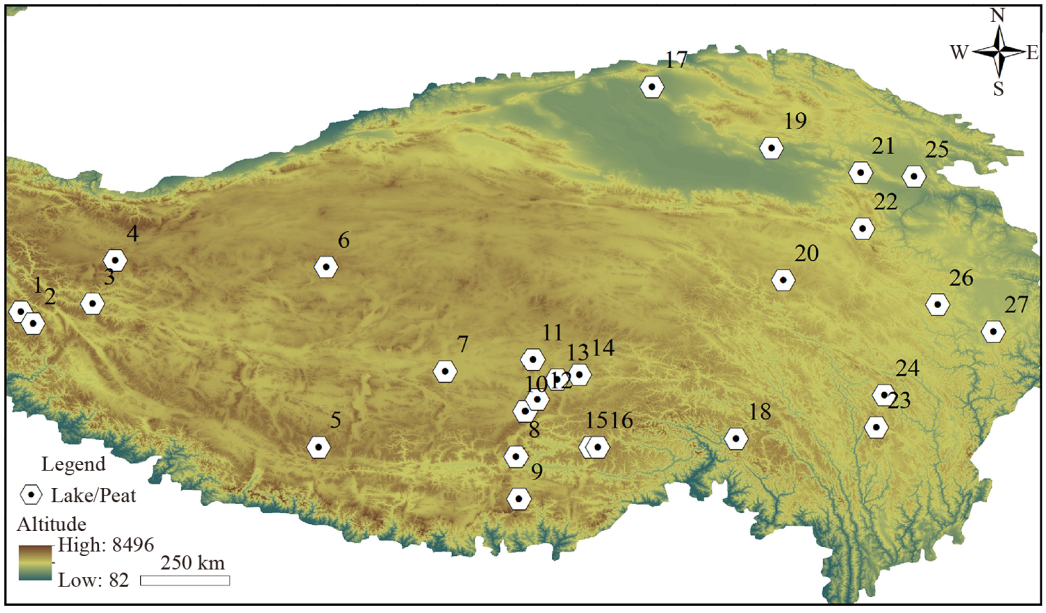

Fig. 1 Spatial distribution of paleoclimatic studies Table 1. Records are numbered from west to east.

Table 1 Paleoclimatic records from the TP arranged from west to east (abbreviations are defined below)

No.	Section	N/(°)	E/(°)	Eleva. /m a.s.l	Time/ cal. ka BP	Dating No.	Using proxies	Dating method	Reference
1	Lake TSO Kar	33.2	78	4527	15−0	32	P	AMS	Demske et al., 2009
2	TSO moriri	32.9	78.3	4512	12−0	6	P	AMS	Leipe et al., 2014
3	Bangong Co	33.4	79.8	4220	14.3−0	19	P	AMS	Van Campo et al., 1996
4	Sumxi Co	34.5	80.38	5058	13−0	6	P D	AMS	Van Campo and Gasse, 1993
5	Peiku Co	29.8	85.5	4595	15−0	8	Ca X	AMS	Du, 2012
6	Buruo Co	34.33	85.7	5170	5.2−0	15	E Gs	AMS	Xu et al., 2019
7	Silin Co	31.7	88.7	4552	5.33−0	13	P	^{137}Cs, ^{210}PbAMS	Sun et al., 1993
8	Pumoyum Co	29.56	90.48	5030	19−0	60	P dC Ca	AMS	Nishimura et al., 2014
	Pumoyum Co	28.5	90.5	5030	19−0	37	P	^{137}Cs, ^{210}Pb, AMS	Lü et al., 2011
9	Chen Co	28.5	90.55	4420	10−3.7	17	S O C/N P Gs C E	AMS	Zhu et al., 2009
10	Nam Co	30.7	90.7	4718	12−0	15	E C/N Gs	AMS	Doberschutz et al., 2014
11	Lake Zigetang	32	90.9	4560	10.6–0	5	P	AMS	Herzschuh et al., 2006
12	Co Ngion	31	91	4515	5.8–0	12	P O C M	AMS	Shen et al., 2008
13	Cuoe Lake	31.5	91.5	4532	10.5–1.6	13	S Gs O dC E C/N	AMS	Wu et al., 2006
14	Ahung Co	31.62	92.06	4575	9.5–4	62	S Gs O dC E C/N	AMS	Morrill et al., 2006
15	Paru Co	29.796	92.352	4845	11−0	7	O L Li	AMS	Bird et al., 2014
16	Hidden Lake	29.8	92.53	4980	12.4−0	4	P	AMS	Tang et al., 2004
17	Sugan Lake	38.85	93.9	2797	7.5−0	8	E O	AMS	Zhang et al., 2022
18	Ren Co	30.01	96.01	4450	20−0	7	P	AMS	Tang et al., 2004
19	Hurleg Lake	37.32	96.9	2817	14.0–0	7	P	AMS	Zhao et al., 2007
20	Koucha Lake	34	97.2	4540	16.4–0	5	P	AMS	Herzschuh et al., 2009
21	Caka Salt Lake	36.7	99.15	3200	17.2–0	10	S M O	AMS	Liu et al., 2008
22	Lake Kuhai	35.3	99.2	4150	18−0	17	P	AMS	Wischnewski et al., 2011
23	Yidun Lake	30.3	99.55	4470	17.3−0	3	P	AMS	Shen et al., 2006
24	Lake Naleng	31.1	99.75	4200	17.6–0	10	S P	AMS	Kramer et al., 2010a, 2010b
25	Lake Qinghai	36.6	100.5	3200	18.0−0	10	P	AMS	Shen et al., 2005
26	Lake Ximencuo	33.38	101.1	4030	13.5−0	13	Gs dC O C/N E	AMS	Zhang and Mischke, 2009
27	Hongyuan Peat	32.7	102.5	3527	11.5−0	11	Gr H	AMS	Yu et al., 2006

Notes: C–carbonate content; C/N–carbon/nitrogen ratios; D–diatoms; dC–carbon isotope; E–elements; Gs–grain size; H-humification; L- leaf wax long-chain; li- lithic flux; M–minerals; O–organic content; P–pollen; S–sediment description; X–X-ray diffraction.

conditions, but these conditions were drier than before on the western, southern and central TP, as well as according to some paleorecords on the south-eastern TP. In contrast, No.17 (Sugan Lake) on the northern TP and No. 19 experienced dry conditions. During the last half of the mid-Holocene (6−4 ka), there were larger regional variations, with a less spatially coherent pattern compared to the early or first half of the mid-Holocene.

During the first half of the late Holocene (4−2 ka), most records showed a continuous moisture decrease except for those areas located on the south-eastern TP and northern TP and No. 19, where the climate remained under wet or relatively wet conditions. In the last 2 ka, almost all paleorecords on the western, southern, central and south-eastern TP experienced the driest conditions during the Holocene, while some records on the north-eastern and northern TP documented moderate conditions.

Then, we apply REOF, and the cumulative variance contribution of the first four modes reached 82.15%, which means that the spatial patterns of moisture evolution of the first four modes are representative of the main moisture pattern on the TP. As shown in Fig. 3, in the leading-order mode, the high positive loading value centers ($\geqslant$ 0.3) are located in the western-southern-central TP (boundary by ~94°E), and the north-eastern and eastern TP including Nos. 22, 23, 26, 27, and 28 (boundary by ~32°N). A low negative loading value center ($\leqslant$ −0.3) is located in the north-eastern TP (No. 20). The remaining modes can be performed in the same manner.

According to the results, the moisture evolution pattern recorded in lake sediment and peat bogs on the TP can be classified into 5 subregions. They are regions A (~28°−

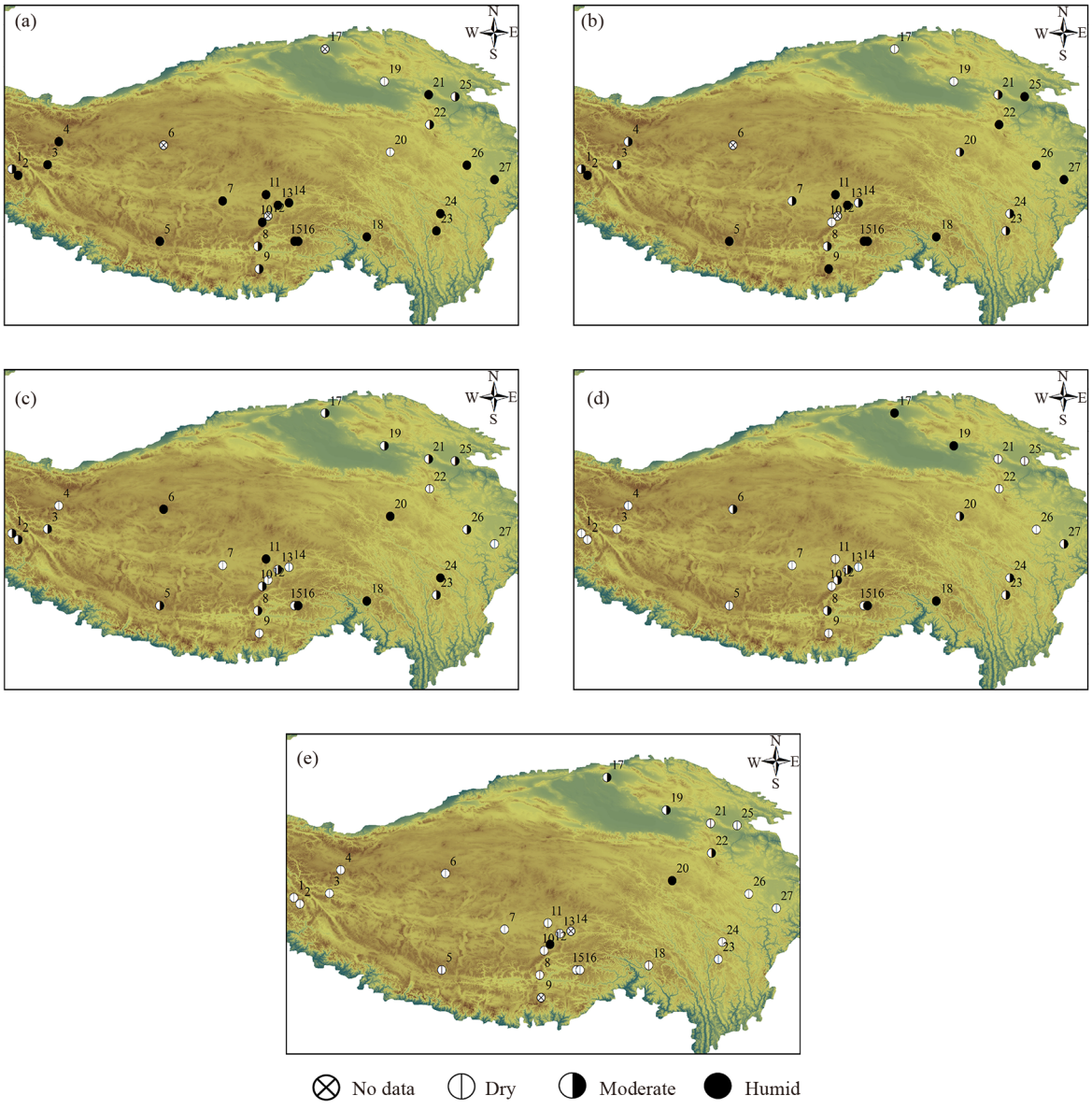

Fig. 2 Spatial moisture changes at each site (site numbers are the same as in Fig. 1) from the TP for time slices of 0–9.5 ka. (a) 9.5–8 ka; (b) 8–6 ka; (c) 6–4 ka; (d) 4–2 ka; (e) 2–0 ka.

35°N, ~78°–94°E; western-southern-central TP), B (~28°–32°N, ~94°–102°E; south-eastern TP), C (~32°–38°N, ~98°–103°E; north-eastern TP), D (~37°–39°N, ~93°–98°E; north-eastern-northern TP) and E (~33°–35°N, ~95°–98°E; north-eastern TP), and there are 16, 3, 5, 2, and 1 paleorecords in each subregion, respectively (Fig. 4 and Figs. S1–S5). According to the synthesized moisture indices, moisture in Region A declined gradually from the early Holocene. In Region B, moisture remained humid during the early Holocene to early-late Holocene. In Region C, there was a wetting trend from 9.5 to approximately 6 ka BP and a persistent drying trend thereafter, with the wettest interval in the middle Holocene. In Region D, there was a wetting trend from the early Holocene to late Holocene. However, in Region E, the moisture index experienced semiwet conditions during the early Holocene and wet conditions during the middle to late Holocene.

3.2 Model results

The time series of summer precipitation evaluated using model grid points that correspond as closely as possible to subregions are compared with the synthesized moisture indices (Fig. 5). The KCM-simulated summer precipitation on the western-southern-central TP, averaged over the region (28°–35°N, 79°–94°E), decreased gradually from the early Holocene to the late Holocene. The model result agreed well with the synthesized moisture index in Region A, with the climatic optimum taking place during the early Holocene (Figs. 2(a) and 5(a)). On the south-eastern TP, modeling data (28°–32°N, 94°–105°E) show

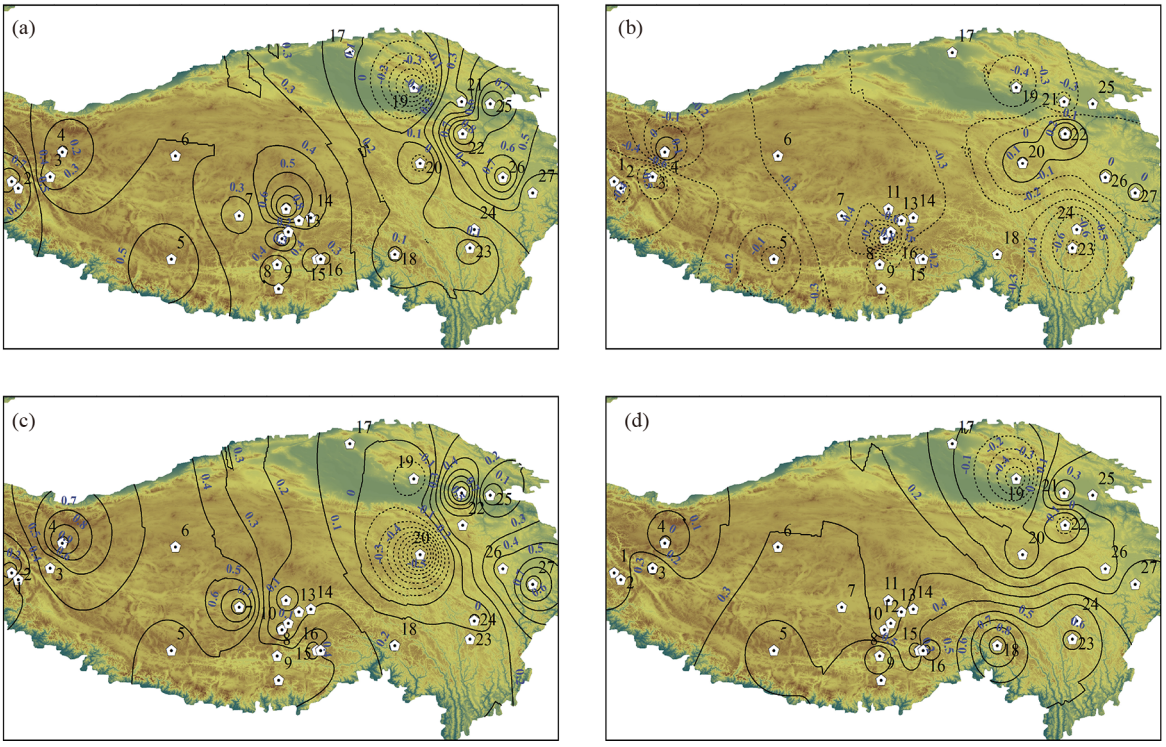

Fig. 3 REOF analysis of moisture evolution recorded at each site (site numbers are the same as in Fig. 1) and the corresponding time series from the TP for time slices of 0−9.5 ka. (a) First mode; (b) second mode; (c) third mode; (d) fourth mode. The blue numbers indicate loading value. The solid black line and dashed black line indicate positive and negative loading values, respectively.

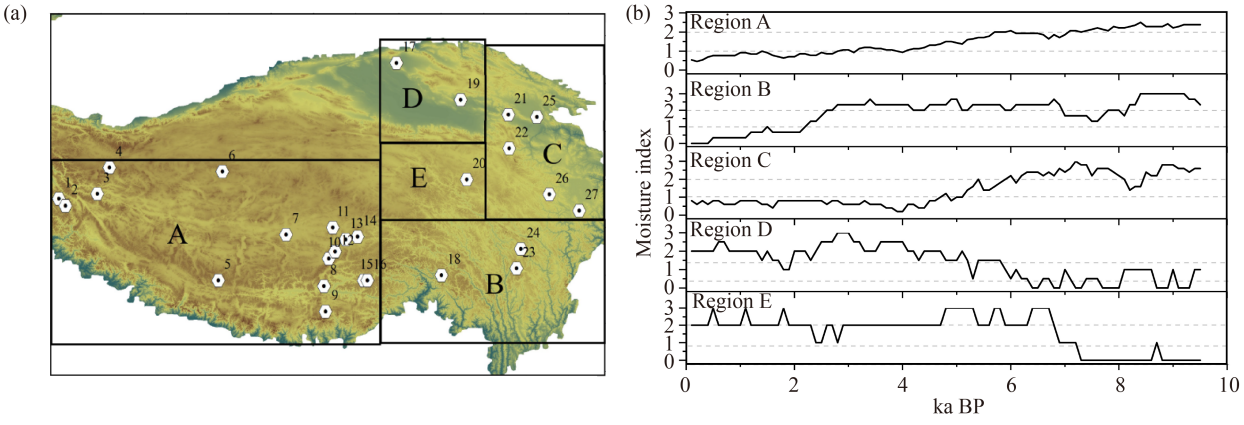

Fig. 4 (a) Map of the division based on REOF analysis; (b) the corresponding synthesized moisture index for each subregion.

that the summer precipitation is high between approximately 6 and 9.5 ka. During the late middle to early late Holocene, summer precipitation is stable and remains at a relatively high level, which resembles the synthesized moisture index in Region B, with maximal summer precipitation occurring in the early and middle Holocene and a relatively moist climate during the late Holocene (Fig. 5(b)). In addition, summer precipitation on the north-eastern TP (35°−43°N, 98°−105°E) shows a wetting trend from approximately 9.5 to ~6.2 ka BP, and summer precipitation declines thereafter, consistent with the synthesized moisture index in Region C (Fig. 5(c)). However, the moisture index in Region D and Region E is inconsistent with the precipitation inferred from nearby model grid points (39°−43°N, 94°−98°E and 32°−35°N, 94°−98°E, respectively) (Figs. 5(d) and 5(e)).

4 Discussion

4.1 Moisture evolution pattern on the TP during the Holocene

The first-order mode emphasizes not only the east–west asymmetry in moisture variation but also the south–north asymmetry on the eastern TP. The south–north asymmetry on the TP, where the separatrix is at approximately 33°N, has been reported by Flohn (1957),

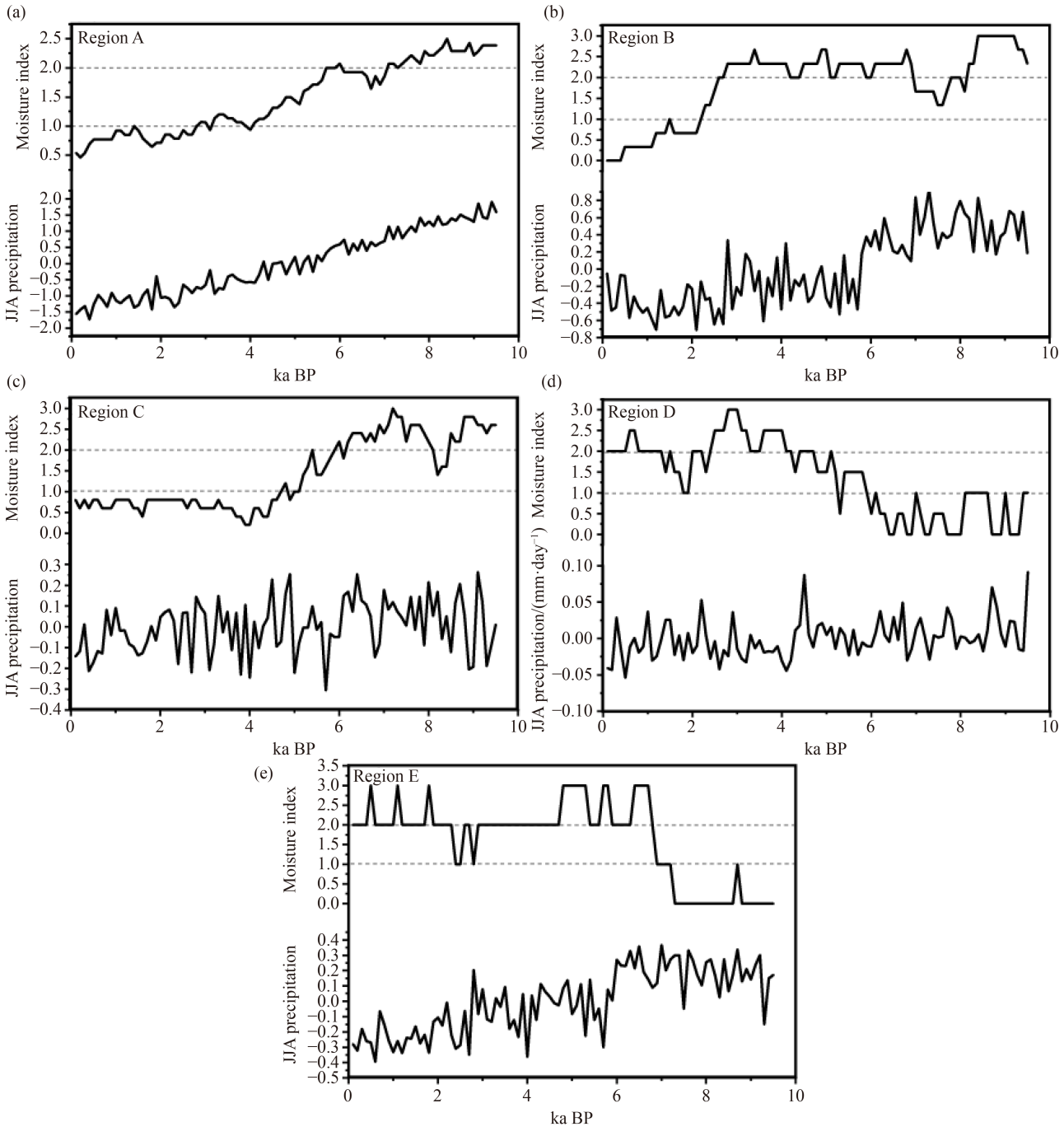

Fig. 5 Moisture changes during the Holocene on the TP from proxy records and climate simulation: (a) synthesized moisture index from Region A (top) and summer (JJA) precipitation nearby (28°–35°N, 79°–94°E) (bottom); (b) same as (a) but in Region B and (28°–32°N, 94°–105°E); (c) same as (a) but in Region C (35°–43°N, 98°–105°E); (d) same as (a) but in Region D and (39°–43°N, 94°–98°E); (e) same as (a) but in Region E (32°–35°N, 94°–98°E).

who pointed out that the Tibetan Highland, with its rolling, rather flat steppe or barren land, acts as an elevated heat source in summer that results in the temperature gradient and baric gradient overturning south of 35°N. In addition, based on the stable isotopes of precipitation of short station records, Tian et al. (2001) insisted that the monsoonal moisture boundary lies at ~35°N. Zhang et al. (2018) confirmed that during the Holocene, the precipitation changes on the north-eastern TP were caused by the interplay between westerlies and the EASM. During the early Holocene, strong mid-latitude westerlies reduced summer precipitation on the north-eastern TP. As a result, the amount of summer precipitation reached its maximum in the mid-Holocene, which was different from paleorecords in other regions over the TP.

In addition, an east–west asymmetry in the monsoon rainfall on the TP remained throughout different periods. Conroy and Overpeck (2011) utilized gridded precipitation data from 1979 to 2009 and confirmed that the south-east region on the TP may not respond to the same monsoon subsystem in the same way as the south-west region. Chen et al. (2015) synthesized the most up-to-date and comprehensive proxy moisture/precipitation records during the past 1000 years in China and showed the opposite phase on the TP in terms of rainfall during the Medieval Climate Anomaly and the Little Ice Age. On the millennial scale, Hudson and Quade (Hudson and Quade, 2013), who used the area surrounded by high shorelines of early Holocene paleolakes to reconstruct paleorainfall patterns during the early Holocene, also confirmed that paleolake areas expanded by approximately 4-fold in the western plateau compared to approximately twofold expansion in the eastern region.

According to our REOF results, the climate change on the northern and north-eastern TP could be divided into 3 subregions: Region C, Region D, and Region E. The amounts of summer precipitation on the north-eastern TP (Region C) were under the control of the mix of EASM and westerlies during the Holocene, which was verified by Zhang et al. (2018). In Region D, Hurleg Lake lies in an arid low-lying basin in the Qaidam Basin and out of the area influenced by the ASM in the modern climate; it showed dry and variable conditions from 9.5 to 5.5 ka and relatively wet and stable conditions after 5.5 ka (Zhao et al., 2007). Additionally, warm and dry conditions with high evaporation/precipitation ratios could be inferred from Sugan Lake from 7.5 to 5.8 ka. Then, the climate became colder with higher lake levels from 5.8 ka on, followed by colder and drier conditions after 3.5 ka BP (Zhang et al., 2022). Both of these lakes recorded humid climate conditions during the middle Holocene and relatively humid conditions during the late Holocene. However, the KCM model data cannot reflect the moisture change, which might be attributed to the fact that in the mid-latitude westerly dominant areas, the dry conditions in the early Holocene seemed to result mostly from changes in winter rather than summer climate (Jin et al., 2014). After comparing the moisture evolution index in Region D with the synthesized Holocene mean moisture index in arid Central Asia, namely, a dry early Holocene, a wetter early to mid-Holocene, and a moderately wet late Holocene (Chen et al., 2008), we infer that this area may have been affected by mainly westerly circulation during the late Holocene under the background of the strengthening westerlies. In Region E, there is only one lake sediment (Koucha Lake). According to the original result, the early Holocene around Koucha Lake was characterized by warmer and drier conditions than today. From approximately 6.6 ka onward, wet and cold conditions dominated in this region, which is contradictory to other paleoclimate records from monsoon-influenced Asia (Herzschuh et al., 2009). In addition, model data cannot capture this pattern. Therefore, strong regionalization of paleoclimate change might be the only reliable explanation. Zhao et al. (2007) also attributed the different moisture evolution to the local terrain after comparing Hurleg sediment with other sediment records.

4.2 Possible forcing mechanism responsible for the discrepancy in moisture inferred from proxy data and model data

4.2.1 Moisture evolution discrepancies induced by circulation configurations during the early Holocene

To determine whether the regional heterogeneity of moisture variability recorded in lake/peat systems on the TP is the consequence of the influence of different climate systems similar to the modern climate, we calculated the East Asian summer monsoon index (EASMI) and Indian summer monsoon index (ISMI) based on the KCM model. The ISMI, which is significantly positively correlated (r = 0.98, n = 95) with summer precipitation in nearby Region A (Fig. 6(a)) and significantly positively correlated (r = 0.81, n = 95) with the rainfall amount nearby Region B (Fig. 6(b)), was defined by boreal summer (JJA) meridional wind anomalies at 850 hPa and 200 hPa over the ISM region (10°−30°N, 71.25°−108.75°E), which confirmed that the ISM was the main control factor for the moisture change in Region A and influenced the moisture change in Region B. The EASMI, which is negatively correlated (r = − 0.62) with summer precipitation in Region B (Fig. 6(c)), was determined by the average boreal summer (JJA) horizontal wind speed at 850 hPa over this area (27.83°−31.54°N, 97.5°−105°E), which suggests that the climate was mainly controlled by the interplay between the EASM and westerlies and the ISM.

Therefore, we conclude that under the different circulation configurations and superposing the terrain influence, the lake/peat records showed a spatial-temporal moisture evolution during the Holocene.

As discussed above, different circulation configurations resulted in regional moisture discrepancies. Here, we analyze the climatologic mean during the Holocene using KCM model data to understand the general circulation pattern and sea level pressure (SLP) pattern (Figs. 7(a) and 7(b)). Westerlies prevailed at 500 hPa in most regions of the TP, similar to the modern climate. At 850 hPa, westerlies still controlled the climate on the northern TP. In addition, strong anticyclonic activity over the Pacific transports water vapor from the Pacific Ocean (EASM circulation) to the eastern TP. On the south-eastern TP, wind vectors from the ISM, which brought water vapor

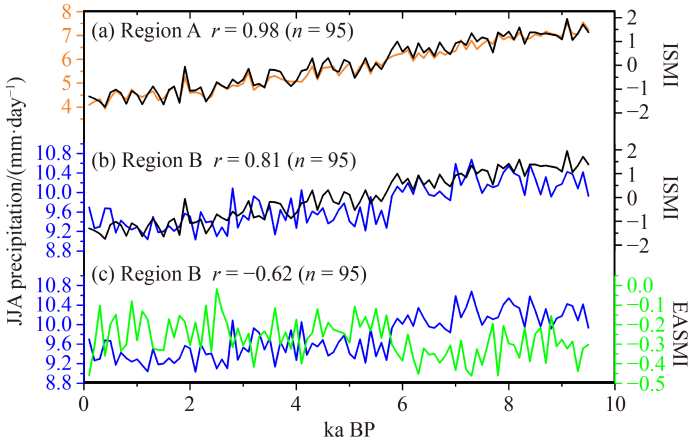

Fig. 6 Comparisons between (a) summer rainfall on the western-southern-central TP (orange line) and the strength of the ISMI (black line); (b) summer rainfall on the south-eastern TP (blue line) and the strength of the ISMI; and (c) summer rainfall on the south-eastern TP and the strength of the EASMI (green line).

from the Indian Ocean, met the wet EASM. In addition to the influence of westerlies on the western-southern-central TP, ISM circulation dominated.

Comparing the early (9.5−8.0 ka)/middle Holocene (8.0−6.0 ka) with the middle/late Holocene (2.0−0 ka), the circulation and SLP patterns are similar (Figs. 7(c)−7(f)). The high-pressure center is on the north-western Pacific, which indicates that the EASM circulation declined gradually from the early Holocene to late Holocene. Meanwhile, water vapor brought forth by a strengthening ISM from the Bay of Bengal and Arabian Sea advanced toward the western, southern, and south-eastern TP, which also indicates a decreasing trend in the ISM circulation. As a result, moisture change inferred from paleoclimatic records in Region A, where the ISM dominated, went through relatively wet conditions in the early Holocene and declined thereafter for the gradually decreasing trend of ISM. In Region B, ISM, EASM, and westerlies influenced the moisture change. Additionally, moisture evolution in Region C and Region E was caused by the interplay between the EASM circulation and the mid-latitude westerlies. In Region D, the climate was under the control of the westerlies. Therefore, the moisture evolution inferred from paleorecords and simulated precipitation was significant and under the control of different circulation and SLP patterns during the Holocene.

However, there are questions regarding why moisture evolution on the TP was asynchronous and why the south-eastern TP remained steady and smooth when the ASM circulations were stronger during the early Holocene than during the middle Holocene, as inferred from paleorecords and simulated precipitation. An alternative explanation, excluding the terrain, may be the natural difference between ISM precipitation and EASM precipitation. ISM precipitation is directly influenced by the intertropical convergence zone, associated with tropical heating and ultimately related to solar radiation (Chao, 2000; Fleitmann et al., 2007). As a result, even though the precipitation in Region A was also influenced by westerlies during the Holocene, the moisture evolution still tracked the ISM circulation. In contrast, EASM precipitation was mainly generated by a frontal system, which formed once the warm and moist air flows met the cold and dry flows (Ding and Chan, 2005). During the early Holocene, the high latitude forcing, i.e., high northern latitude ice volume, weakened land surface temperature and zonal sea–land thermal contrast, and eventually weakened EASM precipitation. This external forcing is accepted by many studies (Li and Xu, 2016; Lu et al., 2019). However, our simulated data did not involve such an external forcing. Therefore, internal feedback is an additional mechanism for consideration. After removing the insolation forcing during the Holocene, the simulated summer precipitation was negatively associated with 850-hPa zonal winds over central-eastern Asia and positively associated with these factors in northern China and the adjacent region (Fig. 8(a)). In addition, simulated summer precipitation on the south-eastern TP was negatively correlated with 850-hPa meridional winds over western central Asia and the north-western Pacific and positively correlated with that over East Asia during the Holocene (Fig. 8(b)). This correlation pattern was similar to that on the north-eastern TP, which resembled a wave-like anomaly pattern in the middle latitudes (Zhang et al., 2018), as shown by the composite difference in the summer wind fields at 850 hPa and 500 hPa between the middle and late Holocene (Figs. 7(e) and 7(f)). This wave-like pattern was beneficial for the southward displacement of cold air and the westward transport of warm water vapor from the north-western Pacific. As a result, anomalous precipitation was generated over the south-eastern TP after this frontal system formation. However, no significant ridge or trough was induced during the early Holocene compared with the middle Holocene (Figs. 7(c) and 7(d)). This circulation pattern

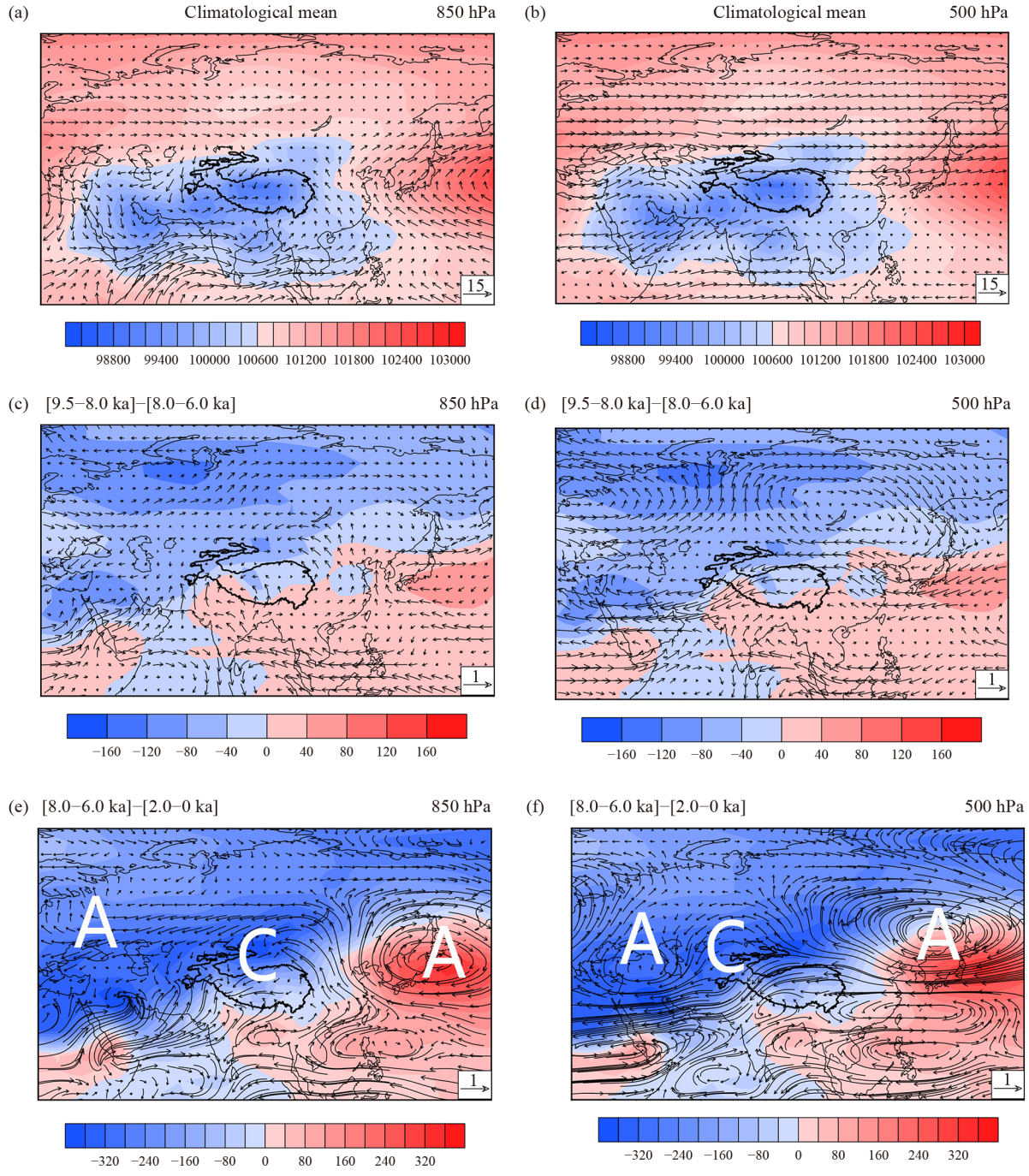

Fig. 7 (a)/(b) Simulated climatological mean SLP and summer wind Felds (m/s) at 850 (500) hPa; (c)/(d) Composite differences in sea level pressure summer wind fields at 850 (500) hPa between the periods of 9.5–8 and 8–6 ka BP; (e)/(f) Composite differences in sea level pressure summer wind fields at 850 (500) hPa between the periods of 8–6 and 2–0 ka BP. 'A' and 'C' indicate anticyclone and cyclone, respectively.

reduced frontal rainfall on the south-eastern TP, which was affected by the interplay between the EASM and westerlies during the early Holocene, despite the enhanced westward transport of warm water vapor from the north-western Pacific, as well as the strong EASM circulation.

Coupling the weakening in ISM circulation and the strengthening in EASM precipitation on the south-eastern TP from the early Holocene to middle Holocene, the moisture evolution on the TP was asynchronous, and on the south-eastern TP, it remained steady and smooth, as inferred from paleorecords and simulated precipitation. In general, with different circulation configurations, especially during the early Holocene and middle Holocene, the moisture evolution inferred from paleorecords and model data showed a spatial discrepancy.

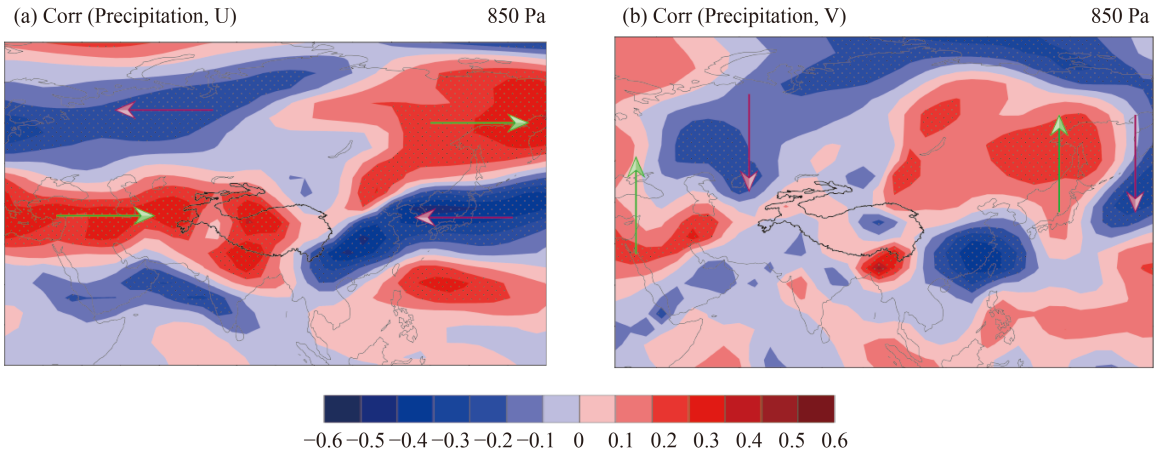

Fig. 8 Correlations between the JJA precipitation averaged on the south-eastern TP (27.83°–31.54°N, 97.5°–105°E) and (a) zonal winds and (b) meridional winds at 850 hPa on millennial timescales (100-year mean and detrended). Black dots indicate correlations that are significant at the 95% confidence level. The arrows indicate the directions of the wind anomalies related to summer precipitation.

4.2.2 Discrepancies in moisture evolution induced by ENSO during the late Holocene

After experiencing relatively weak EASM precipitation during the early Holocene, EASM precipitation reached its maximum at ~6 ka BP and declined thereafter. Meanwhile, the ISM precipitation also decreased gradually in response to the insolation change. However, there has still been a nonuniform climate evolution inferred from paleorecords and simulated precipitation during the late Holocene.

Apart from the increasing intensity of anthropogenic impact during the late Holocene (Zhang et al., 2018), here, we argue that El Niño/Southern Oscillation (ENSO) variability in the equatorial eastern Pacific changes may affect the spatial and temporal variability in precipitation on the TP during the late Holocene. The ENSO index calculated using wintertime (DJF) SST anomalies in Niño 3.4 and averaged every century from KCM data are quite consistent with the Holocene ENSO frequency (Figs. 9(a) and 9(b)) inferred from Laguna Pallcacocha sediment color changes (Moy et al., 2002). The variability, which was relatively weak during the early Holocene and strong during the late Holocene, is also similar to other modeling data. Here, we utilized a composite analysis in the simulated JJA precipitation and 850-hPa wind vectors (m/s) (arrows) between high Niño 3.4 SST years and the climatological mean during the late Holocene (4–0 ka).

When the tropical Pacific Ocean is in a state of El Niño conditions (high Niño 3.4 SST years), the amount of precipitation on the western-southern-central TP decreases with the wind anomalies compared to the climatological mean during the late Holocene. However, regional differences in precipitation are obvious, where the increasing area is on the eastern TP and its adjacent region (Fig. 10).

In fact, the regional differences in summer precipitation in the East Asian region during the Holocene induced by

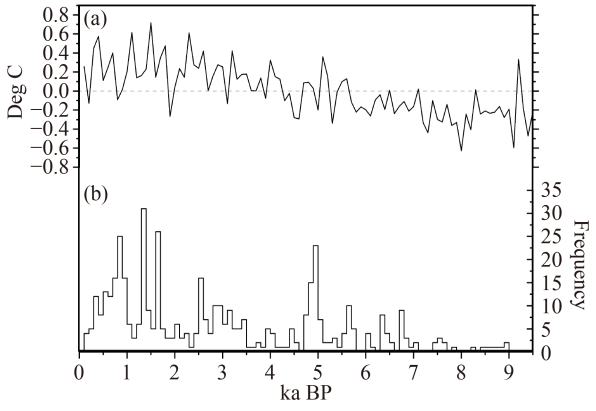

Fig. 9 (a) ENSO index (represented by DJF Niño 3.4 SST of KCM) and (b) the proxy record for Holocene ENSO frequency from Laguna Pallcacocha sediment color changes (Moy et al., 2002).

ENSO variability have been mentioned by many published studies (Jin et al., 2014; Lu et al., 2019). However, because of the complex circulation configurations on the TP discussed above, the precipitation patterns associated with different circulation configurations are more complicated on the TP. First, ENSO-related SST changes can affect the intensity of the western North Pacific (WNP) subtropical high, which is closely related to the EASM strength as well as the position of the EASM rain belt. When El Niño conditions are dominant, with complementary heating in the eastern North Pacific and cooling in the WNP, the WNP subtropical high is enhanced. Therefore, under the background of the enhancement and westward expansion of the WNP subtropical high, more water vapor is transported from the South China Sea toward the middle and lower Yangtze River Valley along the north-west flank of the WNP subtropical high. The enhanced WNP subtropical high during the late Holocene is also supported by Wang et al. (2015), who calculated the position of the West

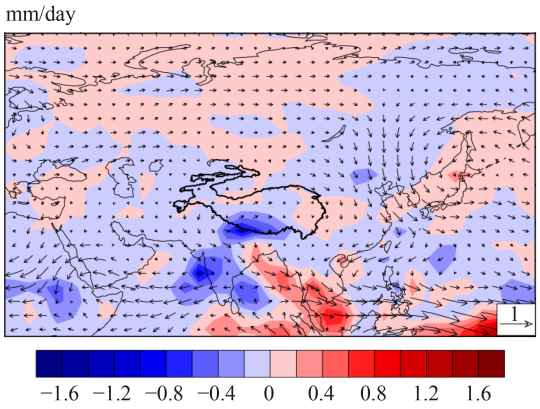

Fig. 10 Composite differences in simulated (HT) total summer (JJA) precipitation and 850 hPa wind vectors (m/s) (arrows) between low and high DJF Niño 3.4 SST years.

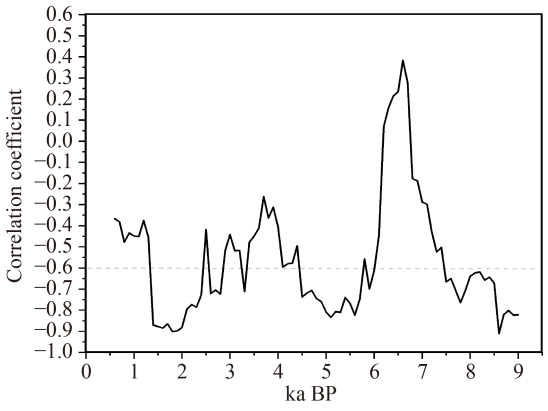

Fig. 11 Running 11-year correlation between the ISM index and ENSO index. The gray line indicates that the correlations are significant at the 95% confidence level.

Ridge Point (WRP) using KCM data and suggested that there is a westward displacement of the WNP subtropical high during the late Holocene. Consequently, precipitation on the eastern TP has increased. Meanwhile, the anomalously strong WNP subtropical high accompanied by low-level south-westerly airflow has weakened the normal south-east monsoon wind over central and northern China, resulting in less precipitation over semiarid northern China (Yang and Lau, 2004; Lu et al., 2019). As a result, precipitation, inferred from paleorecords and simulation data, has become wetter on the eastern TP in response to the El Niño conditions of the late Holocene. These anti-phased responses to ENSO in the EASM area at the millennial-centennial time scales are also similar to those on interannual change and in the precession scale EASM variability from a long-term (284 ka) transient simulation using the fully coupled fast ocean-atmosphere model (FOAM) (Shi et al., 2012).

Second, the millennial-scale ISM tracks the changes in the zonal structure of tropical Pacific SSTs that resemble the spatial patterns of ENSO (Bird et al., 2014), which are also roughly consistent with the modern ISM response to ENSO. However, the influence of ENSO on hydroclimatic variations in the ISM area is also known to be temporally stable (Fig. 11), which reflects the complicated nature of the monsoon dynamics in response to the variability in ENSO on different time scales (Wilson et al., 2010; Xu et al., 2013). Given the anti-phase pattern of summer precipitation in the EASM area under ENSO conditions and the unstable relationship between ISM and ENSO, combined with strong variability during the late Holocene, it is reasonable that the ENSO variability contributes to the spatial-temporal variability in precipitation on the TP.

5 Conclusions

After the critical assessment of the original data and semiquantitative reconstruction, 27 paleoclimate proxy records covering the past 9500 years were selected for detecting the moisture evolution patterns in the last 9.5 ka on the TP. The REOF analysis mainly revealed that the moisture evolution patterns over the TP can be divided into 5 subregions, which are summarized as the south–north asymmetry and east–west asymmetry moisture evolutions.

After comparing the synthesized moisture indices for each subregion with the simulated nearby summer precipitation from KCM data, we confirmed that KCM can be used to detect the possible forcing mechanisms for the regional discrepancies in moisture evolution, and under the different circulation configurations and the superposing influence of terrain, the moisture evolution experienced spatial discrepancies, especially during the early Holocene and middle Holocene. In addition, given the anti-phase in the EASM area under ENSO conditions and the unstable relationship between ISM and ENSO, it is reasonable that the relatively strong ENSO variability during the late Holocene contributed to the spatial-temporal pattern of moisture evolution on the TP.

Supplementary material is available in the online version of this article at http://dx.doi.org/10.1007/s11707-022-1049-3 and is accessible for authorized users.

Acknowledgments This research was supported by the National Natural Science Foundation of China (Grant No. 41775070).

References

An C, Feng Z, Barton L (2006). Dry or humid? Mid-Holocene humidity changes in arid and semi-arid China. Quat Sci Rev, 25(3–4): 351–361

An Z, Colman S M, Zhou W, Li X, Brown E T, Jull A J T, Cai Y, Huang Y, Lu X, Chang H, Song Y, Sun Y, Xu H, Liu W, Jin Z, Liu X, Cheng P, Liu Y, Ai L, Li X, Liu X, Yan L, Shi Z, Wang X, Wu

F, Qiang X, Dong J, Lu F, Xu X (2012). Interplay between the Westerlies and Asian monsoon recorded in Lake Qinghai sediments since 32 ka. Sci Rep, 2(1): 619

An Z, Porter S C, Kutzbach J E, Wu X, Wang S, Liu X, Li X, Zhou W (2000). Asynchronous Holocene optimum of the East Asian monsoon. Quat Sci Rev, 19(8): 743–762

Berger A, Loutre M F (1991). Insolation values for the climate of the last 10 million years. Quat Sci Rev, 10(4): 297–317

Bird B W, Polissar P J, Lei Y, Thompson L G, Yao T, Finney B P, Bain D J, Pompeani D P, Steinman B A (2014). A Tibetan lake sediment record of Holocene Indian summer monsoon variability. Earth Planet Sci Lett, 399: 92–102

Chao W C (2000). Multiple quasi equilibria of the ITCZ and the origin of monsoon onset. J Atmos Sci, 57(5): 641–652

Chen F, Wu D, Chen J, Zhou A, Yu J, Shen J, Wang S, Huang X (2016). Holocene moisture and East Asian summer monsoon evolution in the northeastern Tibetan Plateau recorded by Lake Qinghai and its environs: a review of conflicting proxies. Quat Sci Rev, 154: 111–129

Chen F, Yu Z, Yang M, Ito E, Wang S, Madsen D B, Huang X, Zhao Y, Sato T, Birks H J B, Boomer I, Chen J, An C, Wünnemann B (2008). Holocene moisture evolution in arid central Asia and its out-of-phase relationship with Asian monsoon history. Quat Sci Rev, 27(3–4): 351–364

Chen J, Chen F, Feng S, Huang W, Liu J, Zhou A (2015). Hydroclimatic changes in China and surroundings during the Medieval Climate Anomaly and Little Ice Age: spatial patterns and possible mechanisms. Quat Sci Rev, 107: 98–111

Cheng B, Chen F, Zhang J (2013). Palaeovegetational and palaeoenvironmental changes since the last deglacial in Gonghe Basin, northeast Tibetan Plateau. J Geogr Sci, 23(1): 136–146

Conroy J L, Overpeck J T (2011). Regionalization of present-day precipitation in the greater monsoon region of Asia. J Clim, 24(15): 4073–4095

Demske D, Tarasov P E, Wünnemann B, Riedel F (2009). Late glacial and Holocene vegetation, Indian monsoon and westerlies circulation in the Trans-Himalaya recorded in the lacustrine pollen sequence from Tso Kar, Ladakh, NW India. Palaeogeogr Palaeoclimatol Palaeoecol, 279(3–4): 172–185

Ding Y, Chan J C L (2005). The East Asian summer monsoon: an overview. Meteorol Atmos Phys, 89(1): 117–142

Doberschütz S, Frenzel P, Haberzettl T, Kasper T, Wang J B, Zhu L P, Daut G, Schwalb A, Mausbacher R (2014). Monsoonal forcing of Holocene paleoenvironmental change on the central Tibetan Plateau inferred using a sediment record from Lake Nam Co (Xizang, China). J Paleolimnol, 51(2): 253–266

Dong W, Lin Y, Wright J S, Xie Y, Xu F, Xu W, Wang Y (2017). Indian monsoon low-pressure systems feed up-and-over moisture transport to the southwestern Tibetan Plateau. J Geophys Res Atmos, 122(22): 12140–12151

Du M (2012). A multiproxy record of Asian monsoon variations during the last 15,000 years from Peiku Co, Tibetan plateau. Dissertation for Master Degree. Minneapolis: The University of Minnesota

Fleitmann D, Burns S J, Mangini A, Mudelsee M, Kramers J, Villa I, Neff U, Al-Subbary A, Buettner A, Hippler D, Matter A (2007). Holocene ITCZ and Indian monsoon dynamics recorded in stalagmites from Oman and Yemen (Socotra). Quat Sci Rev, 26(1–2): 170–188

Flohn H (1957). Large-scale aspects of the “Summer Monsoon” in South and East Asia. J Meteor Soc Japan. 35A: 180–186

Gao Y, Cuo L, Zhang Y (2014). Changes in moisture flux over the Tibetan Plateau during 1979–2011 and possible mechanisms. J Clim, 27(5): 1876–1893

He Y, Theakstone W H, Zhang Z, Zhang D, Yao T, Chen T, Shen Y, Pang H (2004). Asynchronous Holocene climatic change across China. Quat Res, 61(1): 52–63

Herzschuh U (2006). Palaeo-moisture evolution in monsoonal Central Asia during the last 50000 years. Quat Sci Rev, 25(1–2): 163–178

Herzschuh U, Kramer A, Mischke S, Zhang C (2009). Quantitative climate and vegetation trends since the late glacial on the northeastern Tibetan Plateau deduced from Koucha Lake pollen spectra. Quat Res, 71(2): 162–171

Herzschuh U, Winter K, Wünnemann B, Li S (2006). A general cooling trend on the central Tibetan Plateau throughout the Holocene recorded by the Lake Zigetang pollen spectra. Quat Int, 154–155: 113–121

Hou J, D’Andrea W J, Liu Z (2012). The influence of ^{14}C reservoir age on interpretation of paleolimnological records from the Tibetan Plateau. Quat Sci Rev, 48: 67–79

Hou J, Tian Q, Liang J, Wang M, He Y (2017). Climatic implications of hydrologic changes in two lake catchments on the central Tibetan Plateau since the last glacial. J Paleolimnol, 58(2): 257–273

Hudson A M, Quade J (2013). Long-term east-west asymmetry in monsoon rainfall on the Tibetan Plateau. Geology, 41(3): 351–354

Jin L, Schneider B, Park W, Latif M, Khon V, Zhang X (2014). The spatial–temporal patterns of Asian summer monsoon precipitation in response to Holocene insolation change: a model-data synthesis. Quat Sci Rev, 85: 47–62

Jin M (2006). MODIS observed seasonal and interannual variations of atmospheric conditions associated with hydrological cycle over Tibetan Plateau. Geophys Res Lett, 33(19): L19707

Kramer A, Herzschuh U, Mischke S, Zhang C (2010a). Late glacial vegetation and climate oscillations on the southeastern Tibetan Plateau inferred from the Lake Naleng pollen profile. Quat Res, 73(2): 324–335

Kramer A, Herzschuh U, Mischke S, Zhang C (2010b). Holocene treeline shifts and monsoon variability in the Hengduan Mountains (southeastern Tibetan Plateau), implications from palynological investigations. Palaeogeogr Palaeoclimatol Palaeoecol, 286(1–2): 23–41

Kutzbach J E (1981). Monsoon climate of the early Holocene: climate experiment with the earth’s orbital parameters for 9000 years ago. Science, 214(4516): 59–61

Leipe C, Demske D, Tarasov P E (2014). A Holocene pollen record from the northwestern Himalayan lake Tso Moriri: implications for palaeoclimatic and archaeological research. Quat Int, 348: 93–112

Li Q, Lu H, Zhu L, Wu N, Wang J, Lu X (2011). Pollen-inferred climate changes and vertical shifts of alpine vegetation belts on the northern slope of the Nyainqentanglha Mountains (Central Tibetan Plateau) since 8.4 kyr BP. Holocene, 21(6): 939–950

Li X, Liu X (2015). Numerical simulation of Tibetan Plateau heating anomaly influence on westerly jet in spring. J Earth Syst Sci, 124(8): 1599–1607

Li Y, Xu L (2016). Asynchronous Holocene Asian monsoon vapor transport and precipitation. Palaeogeography Palaeoclimatology Palaeoecology, 461: 195–200

Liang X, Liu Y, Wu G (2006). Roles of tropical and subtropical land-sea distribution and the Qinghai-Xizang Plateau in the formation of the Asian summer monsoon. Chin J Geophys-Ch, 49(4): 983–992 (in Chinese)

Liu X, Dong H, Rech J A, Matsumoto R, Yang B, Wang Y (2008). Evolution of Chaka Salt Lake in NW China in response to climatic change during the Latest Pleistocene–Holocene. Quat Sci Rev, 27(7–8): 867–879

Lorenz S J, Lohmann G (2004). Acceleration technique for Milankovitch type forcing in a coupled atmosphere-ocean circulation model: method and application for the Holocene. Clim Dyn, 23(7–8): 727–743

Lu F, Ma C, Zhu C, Lu H, Zhang X, Huang K, Guo T, Li K, Li L, Li B, Zhang W (2019). Variability of East Asian summer monsoon precipitation during the Holocene and possible forcing mechanisms. Clim Dyn, 52(1): 969–989

Lü X, Zhu L, Nishimura M, Morita Y, Watanabe T, Nakamura T, Wang Y (2011). A high-resolution environmental change record since 19 cal ka BP in Pumoyum Co, southern Tibet. Chin Sci Bull, 56(27): 2931–2940

Mischke S, Kramer M, Zhang C, Shang H, Herzschuh U, Erzinger J (2008). Reduced early Holocene moisture availability in the Bayan Har Mountains, northeastern Tibetan Plateau, inferred from a multiproxy lake record. Palaeogeogr Palaeoclimatol Palaeoecol, 267(1–2): 59–76

Mischke S, Weynell M, Zhang C, Wiechert U (2013). Spatial variability of ^{14}C reservoir effects in Tibetan Plateau lakes. Quat Int, 313–314: 147–155

Mischke S, Zhang C, Börner A, Herzschuh U (2010). Lateglacial and Holocene variation in aeolian sediment flux over the northeastern Tibetan Plateau recorded by laminated sediments of a saline meromictic lake. J Quaternary Sci, 25(2): 162–177

Morrill C, Overpeck J T, Cole J E, Liu K B, Shen C, Tang L (2006). Holocene variations in the Asian monsoon inferred from the geochemistry of lake sediments in central Tibet. Quat Res, 65(2): 232–243

Moy C M, Seltzer G O, Rodbell D T, Anderson D M (2002). Variability of El Niño/Southern Oscillation activity at millennial timescales during the Holocene epoch. Nature, 420(6912): 162–165

Mügler I, Gleixner G, Günther F, Maüsbacher R, Daut G, Schütt B, Berking J, Schwalb A, Schwark L, Xu B, Yao T, Zhu L, Yi C (2010). A multi-proxy approach to reconstruct hydrological changes and Holocene climate development of Nam Co, Central Tibet. J Paleolimnol, 43(4): 625–648

Nishimura M, Matsunaka T, Morita Y, Watanabe T, Nakamura T, Zhu L, Nara F W, Imai A, Izutsu Y, Hasuike K (2014). Paleoclimatic changes on the southern Tibetan Plateau over the past 19000 years recorded in Lake Pumoyum Co, and their implications for the southwest monsoon evolution. Palaeogeogr Palaeoclimatol Palaeoecol, 396: 75–92

Oldfield F (1999). The Past Global Changes (PAGES) project: a personal perspective. Quat Sci Rev, 18(3): 317–320

Owen L A, Finkel R C, Barnard P L, Ma H, Asahi K, Caffee M W, Derbyshire E (2005). Climatic and topographic controls on the style and timing of late Quaternary glaciation throughout Tibet and the Himalaya defined by ^{10}Be cosmogenic radionuclide surface exposure dating. Quat Sci Rev, 24(12–13): 1391–1411

Park W, Keenlyside N, Latif M, Ströh A, Redler R, Roeckner E, Madec G (2009). Tropical pacific climate and its response to global warming in the Kiel climate model. J Clim, 22(1): 71–92

Peres-Neto P R, Jackson D A (2001). How well do multivariate data sets match? The advantages of a Procrustean superimposition approach over the Mantel test Oecologia, 129(2): 169–178

Richman M B (1986). Rotation of principal components. J Climatol, 6(3): 293–335

Shen C, Liu K B, Morrill C, Overpeck J T, Peng J, Tang L (2008). Ecotone shift and major droughts during the mid-late Holocene in the central Tibetan Plateau. Ecology, 89(4): 1079–1088

Shen C, Liu K, Tang L, Overpeck J T (2006). Quantitative relationships between modern pollen rain and climate in the Tibetan Plateau. Rev Palaeobot Palynol, 140(1–2): 61–77

Shen J, Liu X, Wang S, Matsumoto R (2005). Palaeoclimatic changes in the Qinghai Lake area during the last 18000 years. Quat Int, 136(1): 131–140

Shi Z, Liu X, Cheng X (2012). Anti-phased response of northern and southern East Asian summer precipitation to ENSO modulation of orbital forcing. Quat Sci Rev, 40: 30–38

Sun X, Du N, Chen Y, Gu Z, Liu J, Yuan B (1993). Holocene palynological records in lake Selincuo, northern Xizang. Acta Bot Sin, 35(12): 943–950

Tada R, Zheng H, Clift P D (2016). Evolution and variability of the Asian monsoon and its potential linkage with uplift of the Himalaya and Tibetan Plateau. Prog Earth Planet Sci, 3(1): 4

Tang L, Shen C, Liao J, Yu S, Li C (2004). Climate change on the southeastern Xizang since last glacial maximum. Sci China Ser D Earth Sci, 34: 436–442 (in Chinese)

Tian L, Masson‐Delmotte V, Stievenard M, Yao T, Jouzel J (2001). Tibetan Plateau summer monsoon northward extent revealed by measurements of water stable isotopes. J Geophys Res, 106(D22): 28081–28088

Tschudi S, Schafer J M, Zhao Z, Wu X, Ivy-Ochs S, Kubik P W, Schluchter C (2003). Glacial advances in Tibet during the Younger Dryas? Evidence from cosmogenic ^{10}Be, ^{26}Al, and ^{21}Ne J Asian Earth Sci, 22(4): 301–306

Van Campo E, Cour P, Hang S (1996). Holocene environmental changes in Bangong Co basin (Western Tibet). Part 2: The pollen record. Palaeogeogr Palaeoclimatol Palaeoecol, 120(1–2): 49–63

Van Campo E, Gasse F (1993). Pollen- and diatom-inferred climatic and hydrological changes in Sumxi Co Basin (Western Tibet) since 13000 yr B.P. Quat Res, 39(3): 300–313

Wang N, Jin L, Zhang X (2015). The spatial and temporal variation characteristics of the South Asia high and Western Pacific Subtropical High on millennial time scale. Quaternary Sciences, 35(6): 1425–1436 (in Chinese)

Wang Y, Bekeschus B, Handorf D, Liu X, Dallmeyer A, Herzschuh U (2017). Coherent tropical-subtropical Holocene see-saw moisture patterns in the Eastern Hemisphere monsoon systems. Quat Sci Rev, 169(1): 231–242

Wang Y, Liu X, Herzschuh U (2010). Asynchronous evolution of the Indian and East Asian Summer Monsoon indicated by Holocene moisture patterns in monsoonal central Asia. Earth Sci Rev, 103(3–4): 135–153

Wilson R, Cook R, D'Arrigo N, Riedwyl M N, Evans M N, Tudhope A, Allan R (2010). Reconstructing ENSO: the influence of method, proxy data, climate forcing and teleconnections. J Quaternary Sci, 25(1): 62–78

Wischnewski J, Mischke S, Wang Y, Herzschuh U (2011). Reconstructing climate variability on the northeastern Tibetan Plateau since the last Lateglacial - a multi-proxy, dual-site approach comparing terrestrial and aquatic signals. Quat Sci Rev, 30(1–2): 82–97

Wu D, Ma X, Yuan Z, Hillman A L, Zhang J, Chen J, Zhou A (2022). Holocene hydroclimatic variations on the Tibetan Plateau: an isotopic perspective. Earth Sci Rev, 233: 104169

Wu G, Liu Y, Dong B, Liang X, Duan A, Bao Q, Yu J (2012). Revisiting Asian monsoon formation and change associated with Tibetan Plateau forcing: I. Formation. Clim Dyn, 39(5): 1169–1181

Wu Y, Lücke A, Jin Z, Wang S, Schleser G H, Battarbee R W, Xia W (2006). Holocene climate development on the central Tibetan Plateau: a sedimentary record from Cuoe Lake. Palaeogeogr Palaeoclimatol Palaeoecol, 234(2–4): 328–340

Xu C, Sano M, Nakatsuka T (2013). A 400-year record of hydroclimate variability and local ENSO history in northern Southeast Asia inferred from tree-ring $\delta^{18}O$. Palaeogeogr Palaeoclimatol Palaeoecol, 386: 588–598

Xu T, Zhu L, Lü X, Ma Q, Wang J, Ju J, Huang L (2019). Mid-to late-Holocene paleoenvironmental changes and glacier fluctuations reconstructed from the sediments of proglacial lake Buruo Co, northern Tibetan Plateau. Palaeogeogr Palaeoclimatol Palaeoecol, 517: 74–85

Yang F, Lau K M (2004). Trend and variability of China precipitation in spring and summer: linkage to sea-surface temperatures. Int J Climatol, 24(13): 1625–1644

Yang X, Zhu B, Wang X, Li C, Zhou Z, Chen J, Wang X, Yin J, Lu Y (2008). Late Quaternary environmental changes and organic carbon density in the Hunshandake Sandy Land, eastern Inner Mongolia, China. Global Planet Change, 61(1–2): 70–78

Yu X, Zhou W, Franzen L G, Xian F, Cheng P, Jull A J T (2006). High-resolution peat records for Holocene monsoon history in the eastern Tibetan Plateau. Sci China Ser D Earth Sci, 49(6): 615–621

Zhang C, Mischke S (2009). A Lateglacial and Holocene lake record from the Nianbaoyeze Mountains and inferences of lake, glacier and climate evolution on the eastern Tibetan Plateau. Quat Sci Rev, 28(19–20): 1970–1983

Zhang C, Zhang W, Cheng D, Yang N, Hou X, Li H, Zhang X, Ramamoorthy A (2022). Hydrochemical characteristics and paleoclimate changes recorded from Sugan Lake on the northern boundary of Tibetan Plateau since mid-Holocene. Catena, 217: 106527

Zhang J, Chen F, Holmes J A, Li H, Guo X, Wang J, Li S, Lü Y, Zhao Y, Qiang M (2011). Holocene monsoon climate documented by oxygen and carbon isotopes from lake sediments and peat bogs in China: a review and synthesis. Quat Sci Rev, 30(15–16): 1973–1987

Zhang X, Jin L, Chen J, Lu H, Chen F (2018). Lagged response of summer precipitation to insolation forcing on the northeastern Tibetan Plateau during the Holocene. Clim Dyn, 50(9–10): 3117–3129

Zhang X, Jin L, Jia W (2016). Centennial-scale teleconnection between North Atlantic sea surface temperatures and the Indian summer monsoon during the Holocene. Clim Dyn, 46(9–10): 3323–3336

Zhang Y, Li B, Liu L, Zheng D (2021). Redetermine the region and boundaries of Tibetan Plateau. Geogr Res, 40(6): 1543–1553

Zhang Y, Li B, Zheng D (2002). Adiscussion on the boundary and area of the Tibetan Plateau in China. Geogr Res, 21(1): 1–8

Zhao Y, Yu Z, Chen F (2009a). Spatial and temporal patterns of Holocene vegetation and climate changes in arid and semi-arid China. Quat Int, 194(1–2): 6–18

Zhao Y, Yu Z, Chen F, Ito E, Zhao C (2007). Holocene vegetation and climate history at Hurleg Lake in the Qaidam Basin, northwest China. Rev Palaeobot Palynol, 145(3–4): 275–288

Zhao Y, Yu Z, Chen F, Zhang J, Yang B (2009b). Vegetation response to Holocene climate change in monsoon-influenced region of China. Earth Sci Rev, 97(1–4): 242–256

Zhu L, Lü X, Wang J, Peng P, Kasper T, Daut G, Haberzettl T, Frenzel P, Li Q, Yang R, Schwalb A, Mäusbacher R (2015). Climate change on the Tibetan Plateau in response to shifting atmospheric circulation since the LGM. Sci Rep, 5: 13318

Zhu L, Zhen X, Wang J, Lü H, Xie M, Kitagawa H, Possnert G (2009). A ~30,000-year record of environmental changes inferred from Lake Chen Co, Southern Tibet. J Paleolimnol, 42(3): 343–358